Monthly Notices
of the
ROYAL ASTRONOMICAL SOCIETY

MNRAS **497,** 1895–1903 (2020)
Advance Access publication 2020 July 16

doi:10.1093/mnras/staa2088

Convection and spin-up during common envelope evolution: the formation of short-period double white dwarfs

E. C. Wilson[1]★ and J. Nordhaus[1,2]

[1]*Center for Computational Relativity and Gravitation, Rochester Institute of Technology, Rochester, NY 14623, USA*
[2]*National Technical Institute for the Deaf, Rochester Institute of Technology, Rochester, NY 14623, USA*

Accepted 2020 July 13. Received 2020 July 10; in original form 2020 June 16

ABSTRACT

The formation channels and predicted populations of double white dwarfs (DWDs) are important because a subset will evolve to be gravitational-wave sources and/or progenitors of Type Ia supernovae. Given the observed population of short-period DWDs, we calculate the outcomes of common envelope (CE) evolution when convective effects are included. For each observed white dwarf (WD) in a DWD system, we identify all progenitor stars with an equivalent proto-WD core mass from a comprehensive suite of stellar evolution models. With the second observed WD as the companion, we calculate the conditions under which convection can accommodate the energy released as the orbit decays, including (if necessary) how much the envelope must spin-up during the CE phase. The predicted post-CE final separations closely track the observed DWD orbital parameter space, further strengthening the view that convection is a key ingredient in CE evolution.

Key words: convection – stars: AGB and post-AGB – binaries: general – white dwarfs.

1 INTRODUCTION

Common envelopes (CEs) are short, yet highly critical, phases in the evolution of binary systems (Paczynski 1976). For two main-sequence stars with initial separations $\lesssim$ 5–7 AU, post-main-sequence expansion may result in a CE phase. As the primary star's radius expands during the giant phases, the orbit can destabilize. Engulfment of the secondary by the primary's envelope can occur either directly, or by other processes such as orbital decay via tidal dissipation (e.g. Nordhaus et al. 2010; Ivanova et al. 2013; Nordhaus & Spiegel 2013; Kochanek, Adams & Belczynski 2014; Chen et al. 2017)

Once immersed, the secondary and the primary's core orbit inside a CE. The orbit decays rapidly as energy and angular momentum are transferred to the primary's envelope (Iben & Livio 1993; Nordhaus & Blackman 2006; Nordhaus, Blackman & Frank 2007). Two outcomes can occur: (i) The primary's envelope is ejected leaving a short-period, post-CE binary or (ii) the secondary is destroyed during the CE leaving a single star that had its evolution significantly modified by the secondary (Nordhaus et al. 2011; Guidarelli et al. 2019).

CE evolution is thought to be the primary, though not sole, mechanism for producing the Universe's short-period binaries ($a \lesssim R_\odot$; e.g. Toonen & Nelemans 2013; Canals, Torres & Soker 2018; Kruckow et al. 2018; Fabrycky & Tremaine 2007; Thompson 2011; Shappee & Thompson 2013; Michaely & Perets 2016). Since the CE phase spans only a short fraction of the binary's lifetime, direct detection is difficult. For this reason, identification of CEs rests in their precursor emission (MacLeod, Ostriker & Stone 2018b) and their progeny, e.g. short-period binaries and associated objects such as planetary nebulae (Iben & Livio 1993; Ivanova et al. 2013; Jones 2020).

A widely studied post-CE outcome is that of short-period double white dwarfs (DWDs; Webbink 1984; Iben 1990; Marsh, Dhillon & Duck 1995). DWDs are important binary systems as some are thought to be progenitors of Type Ia supernovae (SNe Ia). In addition, DWDs are potential strong mHz gravitational-wave sources and may be detectable by future missions such as *LISA* (e.g. Iben & Tutukov 1984; Webbink 1984; Ruiter et al. 2010; Brown et al. 2011; Marsh 2011; Ivanova et al. 2013; Kilic et al. 2015)

Observations of DWD candidates have allowed for lengthy compilations of their orbital parameters (Saffer, Liebert & Olszewski 1988; Marsh 1995; Marsh et al. 1995; Holberg et al. 1995; Moran, Marsh & Bragaglia 1997; Maxted et al. 2000, 2002a,b; Napiwotzki et al. 2002; Karl et al. 2003a,b; Morales-Rueda et al. 2005; Nelemans et al. 2005; Kilic et al. 2007a, 2009, 2010; Badenes et al. 2009; Mullally et al. 2009; Kulkarni & Van Kerkwijk 2010; Steinfadt et al. 2010; Vennes et al. 2011; Bours et al. 2014, 2015; Debes et al. 2015; Santander-García et al. 2015; Brown et al. 2016; Hallakoun et al. 2016; Rebassa-Mansergas et al. 2017; Brown et al. 2020). With these data, statistical studies, in combination with binary population synthesis (BPS) studies, have provided an at-large view of the DWD population, often noting that models overpredict the number of observable DWD systems (e.g. Marsh 2011; Ferrario 2012; Toonen et al. 2017; Maoz, Hallakoun & Badenes 2018)

A subset of the observed DWD population is that of extremely low-mass (ELM) white dwarfs (WDs). Typical, single WDs have been observed to follow an initial–final mass relation (IFMR) which describes the correlation between initial stellar mass and final WD mass following a single star's full evolution. A semi-empirical IFMR has been determined for single star systems (Cummings et al. 2018). However, stars in binary systems and especially ELM WDs have masses that are too low when compared to the IFMR. The 'undermassive' nature of these WDs is consistent with the evolution of the star having been interrupted by some binary interaction

★ E-mail: ecw7497@rit.edu

whereby the outer layers of the star have been stripped (Webbink 1984; Iben 1990; Marsh et al. 1995). The interruption of evolution can occur when the primary is on the asymptotic giant branch (AGB) and the proto-WD core is nearly at its IFMR-predicted final mass or the interruption can occur when the primary is on the red giant branch (RGB) and the proto-WD core is just a fraction of the IFMR-predicted final mass (Kilic, Stanek & Pinsonneault 2007b).

Inclusion of convective effects in CEs has been shown to produce M dwarf + WD binaries with periods matching observations, a significant improvement over the results of binary population synthesis studies (Wilson & Nordhaus 2019). Convection transports the energy released by the shrinking orbit to the surface where it is radiated away. This allows the M dwarf to travel deeper into the primary unbinding the envelope, thereby producing subday periods consistent with observations. Convection is also important for the production of SNe Ia as it allows transport of energy and angular momentum outward (Soker 2013).

In this work, we investigate the effect that convection in CEs has on the formation of DWDs. Our initial conditions consist of a WD companion that enters a CE with an evolved star. We calculate the conditions under which convection can accommodate the energy released as the orbit decays including (if necessary) how much the envelope must spin-up during the CE. Under these conditions, we compare the predicted outcomes of CE evolution to the largest observational sample of DWDs to date.

In Section 2, we describe how convection in conjunction with radiative losses from the surface effect the outcomes of CE evolution. In Section 3, we describe the observational sample of DWDs, the stellar models employed, and the physics included in our models. Sections 4 and 5 present the results of our analysis as well as a physical interpretation of the theory and a comparison to the observations. We conclude in Section 6 and comment on future directions.

2 HOW CONVECTION IMPACTS CE EVOLUTION

Global simulation studies have focused on determining the necessary physical processes required to successfully eject the CE. However, these studies have typically neglected effects such as convection and radiation due to computational complexity. Instead, many explore additional energy sources (e.g. recombination, accretion, jets) and longer term processes (Ricker & Taam 2008, 2012; Ivanova, Justham & Podsiadlowski 2015; Nandez, Ivanova & Lombardi 2015; Soker 2015; Kuruwita, Staff & De Marco 2016; Sabach et al. 2017; Glanz & Perets 2018; Grichener, Sabach & Soker 2018; Ivanova 2018; Kashi & Soker 2018; Soker, Grichener & Sabach 2018; Reichardt et al. 2020). However, RGB and AGB stars possess deep and vigorous convective envelopes making convection a necessary ingredient for the physical fidelity of CE simulations.

In lieu of simulations, a widely used, back-of-the-envelope energy argument for estimating how efficiently two stars exchange energy during a CE is often characterized by a constant value, $\bar{\alpha}_{\rm eff}$, typically defined as

$$\bar{\alpha}_{\rm eff} = \frac{E_{\rm bind}}{\Delta E_{\rm orb}}, \tag{1}$$

where $E_{\rm bind}$ is the binding energy of the envelope and $\Delta E_{\rm orb}$ is the change in the companion's orbital energy due to inspiral (e.g. Tutukov & Yungelson 1979; Iben & Tutukov 1984; Webbink 1984; Livio & Soker 1988; De Marco et al. 2011; Iaconi & de Marco 2019). This value is often taken to be a constant, though, in principle, it should functionally depend on the binary parameters and internal structure of the CE. For example, the location and depths of the convective zones were shown to greatly impact where energy can be tapped to drive envelope ejection (Wilson & Nordhaus 2019).

Population synthesis studies, which use an α-prescription that is neither dependent on the internal structure nor the age of the primary, find that very low efficiencies best reproduce observations. These same studies overproduce longer period binaries even though short-period binaries are readily observed in nature (Politano & Weiler 2007; Davis, Kolb & Willems 2010; Zorotovic et al. 2010; Toonen et al. 2017). For DWDs, many studies demonstrate that use of the standard α-prescription does not match observations. In fact, in some cases, the standard α-prescription requires unphysical efficiencies in order to form DWDs (Van Der Sluys, Verbunt & Pols 2006; Woods et al. 2012).

An α-prescription that is physically motivated and dependent on the interior structure of the star may better explain the ejection efficiency within CEs. In CE systems, energy released as the orbit decays can be transported via convection to an optically thin layer of the primary where it is radiated away (MacLeod, Cantiello & Soares-Furtado 2018a; Wilson & Nordhaus 2019). To model convection in CEs, the convective transport time-scale of the primary is compared to the inspiral time-scale. Where the convective transport time-scale is short, compared to the inspiral time-scale, convection can carry orbital energy to the surface where it is lost. In this case, energy would not contribute to unbinding the envelope and, thus, $\alpha_{\rm eff}$ would be consistent with zero in these regions. In the opposite case, where the inspiral time-scale dominates, energy from the decaying orbit can only be used to raise the negative binding energy of the envelope; where this occurs, $\alpha_{\rm eff} = 1$. The convective transport time-scale, inspiral time-scale, and ejection efficiencies are all functions of the radial position, r, inside the primary. The ejection efficiency for the CE phase can then be found by averaging radially-dependent efficiency values in the following way:

$$\bar{\alpha}_{\rm eff} = \frac{\int_{r_{\rm i}}^{r_{\rm f}} \alpha_{\rm eff}[r]{\rm d}E_{\rm orb}[r]}{E_{\rm orb}[r_{\rm f}] - E_{\rm orb}[r_{\rm i}]}. \tag{2}$$

When this physically motivated α-prescription is used, the ejection efficiency and final orbital period are dependent on the size of the surface-contact convective region (SCCR) within the primary. Since the companion can typically travel through this convective region without contributing any energy to unbinding the envelope, a larger SCCR corresponds to a shorter final orbital period, as the companion travels closer to the primary's core before energy can be tapped to drive ejection. The final separation is therefore related to the evolutionary stage of the primary, as the SCCR depth fluctuates with stellar age. In this work, we investigate how the inclusion of convection in CE evolution effects the emergent population of DWDs.

3 METHODS

With a compilation of observed DWDs and their orbital parameters, as well as stellar interior models, we compare the population of DWDs to modelled CE outcomes. A graphical summary of our method is portrayed in Fig. 1, with panels (a), (b), and (c) corresponding to Sections 3.1, 3.2, and 3.3, respectively.

3.1 Observations

To date, many DWDs have been observed and characterized primarily via radial velocity and/or transit methods (Saffer et al. 1988; Marsh

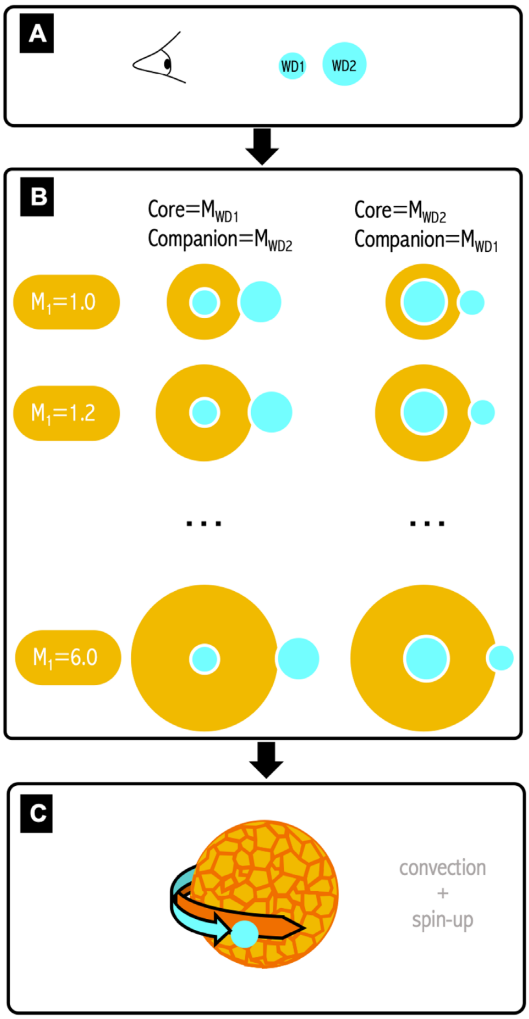

Figure 1. A cartoon of the method employed in this paper, in three panels. Panel (a): A list of DWD observations is used, which include WD masses and periods. Separations are estimated assuming circular orbits. Panel (b): Using stellar evolution models, we match the modelled core mass and the modelled CE companion to both of the observed/derived values for stellar models of primaries ranging from 1.0 to 6.0 $M_\odot$. Panel (c): CE evolution includes convective effects as in Wilson & Nordhaus (2019) and spin-up of the envelope.

1995; Marsh et al. 1995; Holberg et al. 1995; Moran et al. 1997; Maxted et al. 2000, 2002a,b; Napiwotzki et al. 2002; Karl et al. 2003a,b; Morales-Rueda et al. 2005; Nelemans et al. 2005; Kilic et al. 2007a, 2009, 2010; Badenes et al. 2009; Mullally et al. 2009; Kulkarni & Van Kerkwijk 2010; Steinfadt et al. 2010; Vennes et al. 2011; Bours et al. 2014, 2015; Debes et al. 2015; Santander-García et al. 2015; Brown et al. 2016; Hallakoun et al. 2016; Rebassa-Mansergas et al. 2017; Brown et al. 2020). Our sample consists of 141 DWD systems, each of which contain observed masses, the corresponding orbital periods, and statistical constraints on the secondary masses. We determine a separation for each system assuming the orbits are circular (Fig. 1, panel a).

3.2 Stellar models

We use MODULES FOR EXPERIMENTS IN STELLAR ASTROPHYSICS (MESA, release 10108), an open-source stellar evolution code, to produce detailed, spherically-symmetric stellar interior models (Paxton et al. 2011, 2018).[1] The full evolution of the star is calculated for zero-age main-sequence masses from 1.0 to 6.0 $M_\odot$ in increments of 0.2 $M_\odot$ with solar metallicity ($Z = 0.02$). To match the semi-empirical initial–final mass relationship (IFMR) of Cummings et al. (2018), we adopt a Reimers mass-loss prescription with $\eta_R = 0.7$ on the RGB and a Bloecker mass-loss prescription with $\eta_B = 0.15$ on the AGB (Reimers 1975; Bloecker 1995). Given these mass-loss coefficients, our evolutionary models match the observationally derived IFMR within the measured errors (Cummings et al. 2018).

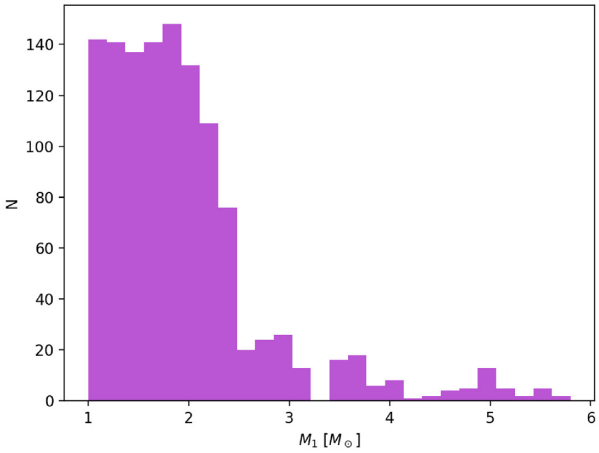

Figure 2. The frequency of primary mass values from which the cores are modelled. No IMF is assumed from which to draw our data; this is effectively an IMF from which our data are drawn. Models were selected from a suite of primary masses (1.0–6.0 $M_\odot$) at a time in each primary's evolution when the mass of the core equals the mass of an observed DWD component within 0.02 $M_\odot$.

For each WD mass in our observational sample of DWDs, we determine the time in each modelled star's evolution at which the core mass matches the observed WD mass to within 0.02 $M_\odot$ from a suite of primary mass models, ranging from 1.0 to 6.0 $M_\odot$. This is depicted in Fig. 1, panel (b). With several initial mass primary models mapped to each observed system, the radius of the convective boundary of each modelled primary was found for this set of initial masses. We do not use any formal initial mass function (IMF). Rather, we draw from all masses in our range, equally. This approach generates an initial mass distribution from the primaries, which produced cores that match DWD observations. This distribution is shown in Fig. 2. We note that while the core mass for each model monotonically increases in time, several higher initial mass ($M \geq 2.6\,M_\odot$) MESA models display a sharp, step-like discontinuity in core mass. In these cases, the core mass jumps from 0 to ~8–10 per cent of the primary mass in a single time-step, preventing a match to observations for WDs with masses less than ~8–10 per cent of the initial mass primary. In particular, the observed ELM WDs can only be matched by MESA models that exhibit continuous core growth (i.e. $M < 2.6\,M_\odot$).

3.3 Modelling the CE with convection and spin-up

For each observed DWD system, two corresponding CEs were modelled: (i) the more-massive WD as the companion and the less-massive WD as the core mass, and (ii) the less-massive WD as the

[1] MESA is available at http://mesa.sourceforge.net.

companion and the more-massive WD as the core mass.[2] These two modelled systems were then iterated through several initial-mass primaries as shown in Fig. 1, panel (b).

Convective effects of the primary were taken into account by comparing the inspiral time-scale,

$$t_{\rm inspiral}[r] = \int_{r_{\rm i}}^{r_{\rm shred}} \frac{\left(\frac{{\rm d}M}{{\rm d}r} - \frac{M[r]}{r}\right)\sqrt{v_r^2 + (\bar{v}_\phi[r]^2 + c_{\rm s}[r]^2)^2}}{4\xi\pi G m_{\rm comp} r\,\rho[r]}{\rm d}r \quad (3)$$

(Nordhaus & Blackman 2006), to the convective transport time-scale,

$$t_{\rm conv}[r] = \int_{r_{\rm i}}^{R_\star} \frac{1}{v_{\rm conv}[r]}{\rm d}r \quad (4)$$

(Grichener et al. 2018), where r_i is the initial radial position and $r_{\rm shred}$ is the tidal shredding radius of the companion, approximated as $r_{\rm shred} \simeq R_{\rm comp}\sqrt[3]{2M_{\rm core}/m_{\rm comp}}$ (Nordhaus et al. 2007), where $R_2 = r_{\rm WD}$, estimated via the WD mass–radius relation (Chandrasekhar 1933; Hamada & Salpeter 1961; Wood 1990, 1994). The velocity terms v_r, $c_{\rm s}$, v_ϕ, $v_{\rm env}$, and $v_{\rm conv}$ are the radial velocity of the companion, the sound speed, the Keplerian velocity, envelope velocity, and the convective velocity, respectively. The relative velocity of the companion to the velocity of the envelope is given by $\bar{v}_\phi = v_\phi - v_{\rm env}$. We use $\xi = 4$ to account for the geometry of the secondary's wake within the primary (Park & Bogdanović 2017). M is the enclosed stellar mass and ρ denotes the primary's density. Terms that are shown with an r in square brackets are radially dependent.

Where the convective transport time-scale is less than the inspiral time-scale, energy liberated from the decaying orbit can be carried to the surface via convective eddies where it is lost from the system via radiation. Note that in this regime, we assume the primary's radius does not appreciably expand and thus the liberated orbital energy does not contribute to unbinding the CE. For regions where the convective transport time-scale is long compared to the inspiral time-scale, energy must be deposited locally in the gas and thus can only be used to raise the negative binding energy of the envelope. The orbit continues to shrink until the envelope is either unbound, leaving a post-CE DWD, or the companion tidally disrupts inside the CE, leaving a single star whose evolution has been significantly modified.

Convection in CEs is an important physical effect to investigate as RGB and AGB stars have deep and vigorous convective envelopes. In addition to transporting energy, convection also acts to distribute energy throughout the envelope. While the depth of the convective region changes on hundred-year time-scales, the inspiral time-scales are short (often $\lesssim$1 yr, but at most $\sim$30 yr). Thus, we perform an analysis of the effects of convection for a single snapshot in the primary's evolution.

In addition to convection, we also consider spin-up of the envelope during CE evolution as simulations of CEs have shown significant transfer of angular momentum from the orbit to the gas (Ricker & Taam 2012; Chamandy et al. 2018; MacLeod et al. 2018b). As RGB/AGB stars are slow rotators, we assume that each primary is initially stationary. As the companion inspirals through the primary, the envelope velocity, $v_{\rm env}$, can increase as it begins to spin until it reaches co-rotation, where $v_{\rm env} = v_\phi$ and orbital decay is halted. In order for convection to transport the companion's orbital energy, the maximum luminosity that subsonic convection can accommodate,

$$L_{\rm conv,max}[r] = 4\pi\rho[r]r^2 c_{\rm s}[r]^3 \quad (5)$$

(Quataert & Shiode 2012; Shiode & Quataert 2014; Sabach et al. 2017), must be greater than the drag luminosity,

$$L_{\rm drag}[r] = \xi\pi R_{\rm acc}^2\rho[r](v_\phi[r] - v_{\rm env})^3, \quad (6)$$

where $R_{\rm acc}$, the accretion radius, is given by

$$R_{\rm acc} = \frac{2Gm_{\rm comp}}{(v_\phi[r] - v_{\rm env})^2 + c_{\rm s}[r]^2} \quad (7)$$

(Nordhaus & Blackman 2006). If the relative velocity between the orbit, v_ϕ, and the envelope, $v_{\rm env}$, is reduced, the $L_{\rm drag} \leq L_{\rm conv,\,max}$ constraint is more readily met since the inspiral time-scale increases. The inspiral time-scale may be increased such that the convective transport time-scale becomes dominant, thus allowing the companion to travel deeper into the primary before contributing energy to unbind the envelope, thereby decreasing the ejection efficiency. When $L_{\rm drag} \leq L_{\rm conv,\,max}$, the nature of convection is unchanged; if the opposite is true ($L_{\rm drag} > L_{\rm conv,\,max}$), convection will transition to the supersonic regime where orbital energy can converted to kinetic energy via shocks, thereby making the primary's envelope less bound.

For the orbital energy released during inspiral through the convective zone to be fully transported and radiated away, some amount of spin-up of the envelope may be required to satisfy the luminosity condition. The amount required is calculated by first representing the relative velocity of the two bodies as a fractional velocity: $v_\phi[r] - v_{\rm env} = \beta v_\phi[r]$, which is then substituted into equation (6). The drag luminosity and the maximum luminosity that convection can accommodate are then equated, i.e. $L_{\rm drag} = L_{\rm conv,\,max}$. By setting $r = r_{\rm SCCR}$, the base of the SCCR[3] the solutions for β can be found by solving the following fourth-order equation:

$$v_\phi[r]^4\beta^4 - \frac{\xi G^2 m_{\rm comp}^2 v_\phi[r]^3}{r^2 c_{\rm s}[r]^3}\beta^3 + 2v_\phi[r]^2 c_{\rm s}[r]^2\beta^2 + c_{\rm s}[r]^4 = 0. \quad (8)$$

Note that because this equation is evaluated $r = r_{\rm SCCR}$, the solutions are the spin-up values at the base of the convective zone; if the region spanning from the base of the convective zone to the surface were rotating at this value, the luminosity condition, $L_{\rm drag} \leq L_{\rm conv,\,max}$ would easily be met.

For this analysis, only real roots of the above equation are considered. For systems with $\beta = 0$, the companion and the stellar envelope are fully co-rotating. For systems with $\beta = 1$, the stellar envelope is stationary. We assume that the envelope is initially stationary, requiring the envelope to spin-up from stationary ($\beta = 1$) to some velocity ($\beta \to 0$) during the companion's inspiral; the real β value closest to unity without exceeding it is used as the solution for each given system. The fraction of Keplerian speed taken on by the envelope is represented by $1 - \beta$ (e.g. $\beta = 0.7$ has an envelope spun-up to 30 per cent co-rotation), which is equivalent to $v_{\rm env}/v_\phi$.

To determine if the companion has deposited sufficient energy to unbind the envelope, we compare the primary's binding energy, $E_{\rm bind}$, to the companion's change in orbital energy, $\Delta E_{\rm orb}$, with an efficiency, $\bar{\alpha}_{\rm eff}$, where $\bar{\alpha}_{\rm eff}$ can be calculated via equation (2). We consider the envelope to be ejected, and therefore the final orbital

[2]We take the mass of the WD and the mass of the primary's core to be constant during CE evolution. The accretion rate on to a WD at the Eddington limit is given by $\dot{M}_{\rm Edd} \simeq 3 \times 10^{-5}\,(R/R_{\rm WD})\ {\rm M}_\odot\ {\rm yr}^{-1}$. Even if the CE were to last 10^3 yr, accretion would only increase the WD's mass by 3 per cent.

[3]The surface-contact convective zone (SCCR) radius, $r_{\rm SCCR}$, is defined as the radius from the centre of the primary to the base of the convective region that extends to the stellar surface.

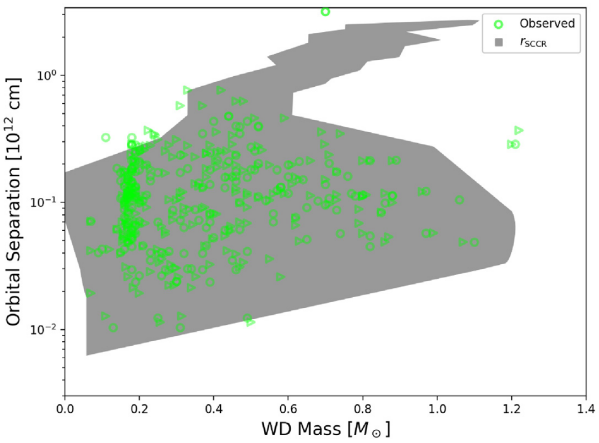

Figure 3. Comparison of observed DWD orbital parameters (green circles) and parameter space filled by the distance from the stellar core to the convective boundary (shaded grey). Each component mass of the DWD system is plotted individually. The parameter space filled by the models closely resembles the parameter space filled by the observed data. This correlation highlights the strong connection between convection in CEs and the post-CE DWD population.

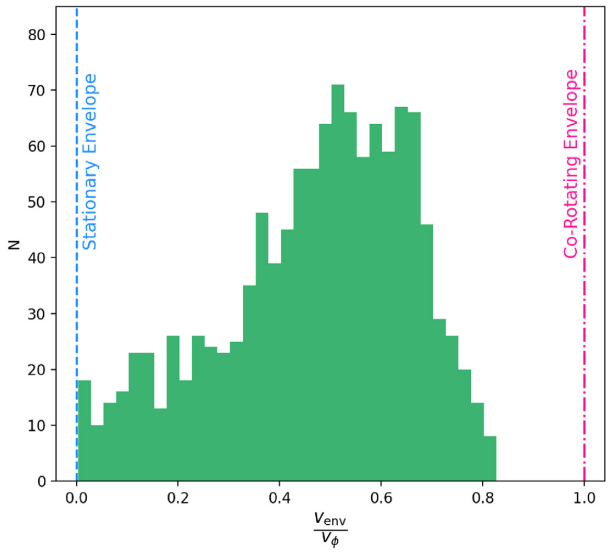

Figure 4. Frequency of v_{env}/v_ϕ values in the total population of initial mass models. The v_{env}/v_ϕ value is the fraction of co-rotation necessary for the inspiral time-scale to increase enough for the maximum convective luminosity to exceed the drag luminosity, thus enabling convection to carry the energy to the surface. It falls off sharply after a peak at $v_{env}/v_\phi = 0.7$, indicating that an envelope spin-up of >70 per cent of Keplerian is not commonly necessary.

separation of the pair to be, where the change in orbital energy is equal to the binding energy.

4 POST-CE ORBITAL SEPARATIONS

4.1 Convection alone

During CE evolution, convection can transport the released orbital energy of the companion to the primary's optically-thin surface where the energy can be radiated away (Soker 2013; MacLeod et al. 2018a; Wilson & Nordhaus 2019). This allows the companion to inspiral deep into the primary before reaching a region where convection can no longer sufficiently transport energy to the surface. Once the companion reaches this region, orbital energy cannot be radiated away and must contribute unbinding the envelope. This often occurs at the base of the convective zone where the inspiral time-scale is greater than the convective transport time-scale. The orbital energy liberated at the base of the convective zone is greater than the binding energy for many systems, and thus the envelope is often ejected here.

In many cases, the inclusion of convection predicts the post-CE binary's final separation to be the distance between the primary's core and convective boundary, r_{SCCR}, and is consistent with the subday periods of post-CE, M dwarf + WD pairs (Wilson & Nordhaus 2019). Given the observed population of short-period DWDs, we compare r_{SCCR} to the observed DWD separations, a_{obs}. Because the same core mass can be produced via many different primary mass stars, each system cannot be mapped directly to a single model. Instead, for this comparison, each WD in the pair is reported with its a_{obs} separately and is compared to the population of stellar models with the same core mass. Across all observed DWD masses, we find a correlation between a_{obs} and r_{SCCR}, underscoring a potential relationship between short-period binaries and convective properties of the primary.

The correlation between a_{obs} and r_{SCCR} can be seen in Fig. 3. The 282 green points represent each WD in the set of observed DWDs (141 pairs). The grey shaded region is the space filled by the r_{SCCR} values of models with the same core mass as the observed DWD components. This novel correlation may indicate that WDs tend to halt their inspiral (i.e. eject the envelope) shortly after exiting the convective zone. To determine under what conditions the engulfed WD would eject the envelope of the primary at the base of the convective zone, we included spin-up in our CE model which we discuss below.

4.2 Convection and spin-up

In order to eject the envelope at the base of the convective zone, the following criteria must be met: (i) The orbital energy released as the companion exits the convective zone must be in excess of the binding energy, and (ii) the maximum luminosity that convection can accommodate must be greater than the drag luminosity throughout the SCCR. Since angular momentum is also transferred from the orbit to the gas, any spin-up of the envelope will lengthen the inspiral time-scale. This, in turn, relaxes the conditions for convection to transport energy to the surface.

Since there is a limit to how much energy can be transported by subsonic convection, we calculate the amount of spin-up necessary to ensure that $L_{drag} \leq L_{conv,\,max}$. At the SCCR, we allow the envelope to spin-up to some fraction of the Keplerian speed as determined by equation (8). While this equation yields four solutions, we choose the solution closest to unity without exceeding it. When $\beta = 1$, the envelope is stationary and thus as the envelope spins up, β decreases until the envelope is in co-rotation with the orbit, i.e. $\beta = 0$. The value $1 - \beta$ is equivalent to the ratio v_{env}/v_ϕ.

For all but two modelled cases of our observed systems, there is a real, physical ($0 < \beta < 1$) solution. However, we note that there are an additional two systems that lack a matching MESA model altogether. The frequency of v_{env}/v_ϕ values peaks between 0.5 and 0.7, before sharply dropping off. There are very few systems with $v_{env}/v_\phi > 0.8$, indicating that it is rarely necessary for the envelope to reach 80 per cent of the Keplerian speed. A histogram of v_{env}/v_ϕ values for the simulated initial systems is seen in Fig. 4.

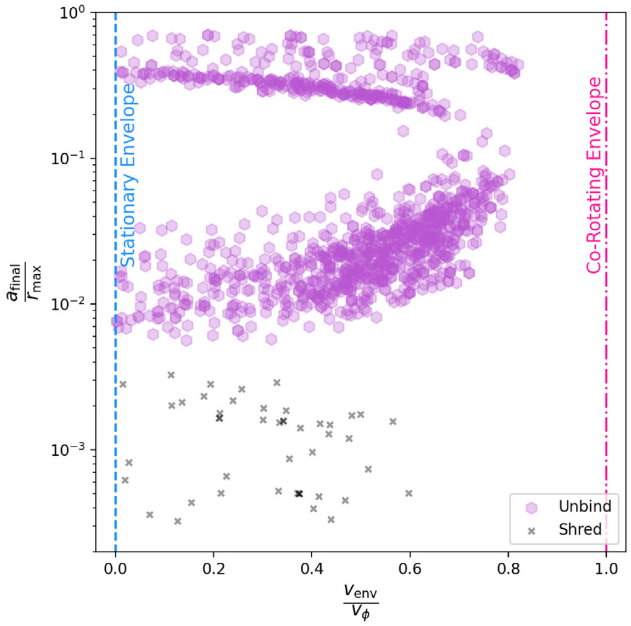

Figure 5. Final system orbital separation normalized to the radius of the primary with spin-up. Purple hexagons show systems where the companion has enough energy to unbind the envelope. Black Xs show systems where the companion shreds within the envelope. Most systems that shred and approximately half of systems that unbind have unphysical solutions for β and are not plotted within these bounds.

4.3 Unbinding the envelope

Though we do not formally draw from an IMF, we note how many post-CE, short-period binaries emerge from our initial mass pairings. The initial-mass primaries coupled with WD companions are modelled via a convective CE with an envelope spun-up to their calculated v_{env}/v_ϕ. Of all modelled systems, 78 per cent have sufficient energy from the inspiraling companion to unbind the primary's envelope; the remainder tidally disrupt within the primary leaving binary-modified, single stars. In Fig. 5, the final orbital separation is shown, normalized to the radius of each initial mass primary, in purple hexagons. The systems that tidally shred are marked at their shredding radii with black Xs. A smaller a_{final}/r_{max} corresponds to a shorter orbital period as the companion has travelled deeper into the envelope of the primary. The spin-up values for each system are calculated via equation (8).

5 DISCUSSION

5.1 Convective, spin-up model matches observations

The correlation in parameter space displayed between the observed orbital separation versus observed WD mass and the modelled convective boundary versus modelled core mass (see Fig. 3) is consistent with the ejection efficiency theory described in Wilson & Nordhaus (2019). There is a degeneracy in initial mass of the modelled cores, and, thus, a closer relationship cannot be determined. A given core mass can be modelled by up to 26 initial primary masses (1.0–6.0 $M_\odot$). Since core masses grow at varying rates for different primary masses, the state of the star when its evolution is interrupted, and therefore the location of the convective boundary depends on the mass of the primary. The depth of the convective zone can also change on time-scales of the order of $\sim 10^2$ yr for a single star.

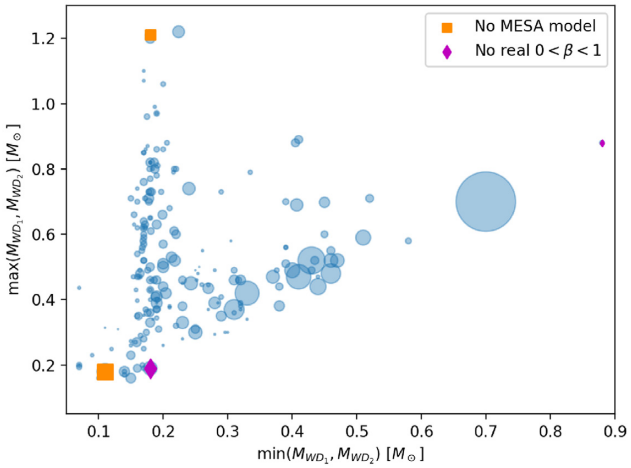

Figure 6. Mass-mass space of each observed DWD system; marker size corresponds to the orbital period. The orange squares mark the two systems that were not modelled due to the lack of MESA models with core masses that matched observed WD masses. The magenta diamonds mark the two systems with only imaginary β values. All four systems without a solution are on the periphery of parameter space.

Though the modelled core masses match the observed core masses within a few per cent, this variability combined with the lack of an IMF make this correlation intriguing but require future study for more robust conclusions to be drawn.

As described in Section 4.2, there is a solution for every initial mass system that was modelled[4] with only two exceptions. This means that for each observed DWD system, there is a reasonable scenario where convection and spin-up will allow the envelope to be ejected at the base of the convective zone. Fig. 6 displays all of the observed DWD systems in the mass–mass space as well as the two systems that do not have a β solution, and the two systems that do not have a corresponding MESA model. All four lie on the periphery.

Our predicted DWD separations closely match those observed (see Fig. 7). The green circles represent known DWD systems and are the same as those in Fig. 3. The colourful squares represent the DWD components and are coloured by the calculated spin-up value. The parameter space filled by observations is also filled by models. The overrepresentation of very short period ($\lesssim 10^{10}$ cm) systems may be due to the lack of sampling from an IMF.

5.2 Spin-up and mass ratio

There is a correlation between the mass ratios of the initial systems, m_{comp}/M_1, and the amount of spin-up necessary such that the maximum convective luminosity is greater than the drag luminosity. As the mass ratio increases, the β value decreases, i.e. the amount of spin-up necessary to meet the luminosity inequality increases (since $v_{env}/v_\phi = 1 - \beta$). This relationship is shown with blue points in Fig. 8.

The mass ratio of the initial system can also be mathematically related to β by making the approximation $v_\phi \simeq c_s$, a reasonable assumption given that the Mach number, $\mathcal{M}$, is of order unity in these systems except near the stellar surface. For three primary models, $\mathcal{M}$ versus r is shown in Fig. 9. When the Keplerian velocity and the

[4]Note that two systems were not modelled as no MESA core was able to match the mass of the observed WD to within 0.02 $M_\odot$.

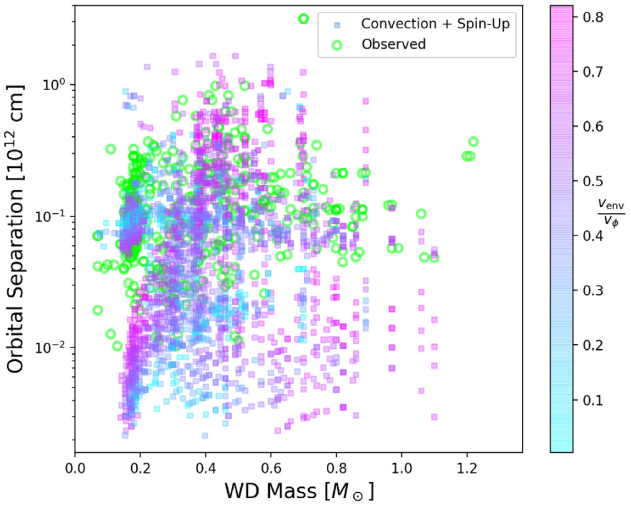

Figure 7. A comparison of observed DWD orbital separations and final separations of modelled CEs with convection and spin-up. The v_{env}/v_ϕ values are shown in a colour gradient from $v_{env}/v_\phi = 0$ (stationary envelope) in cyan to $v_{env}/v_\phi = 1$ (co-rotating envelope) in magenta. The modelled systems with convection and spin-up match observed systems. There is an overrepresentation of very short period ($<10^{10}$ cm) systems, which may be due to the lack of an IMF in this work.

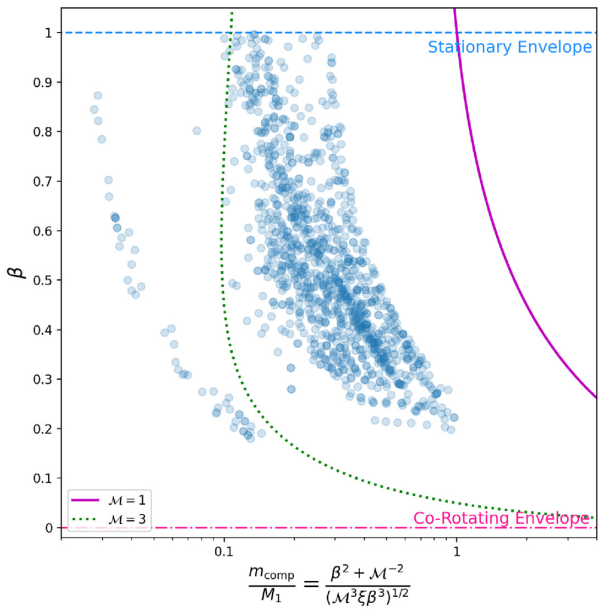

Figure 8. The β value ($1 - v_{env}/v_\phi$) as a function of corresponding mass ratio of modelled systems. The mass ratio is calculated to always be less than unity and β is calculated with use of model parameters as described in equation (8). The two curves follow β as a function of the mass ratio and the Mach number, $\mathcal{M}$; $\mathcal{M} = 1$ is shown by the solid magenta curve and $\mathcal{M} = 3$ is shown by the dashed green curve. These curves bound the modelled data with few exceptions and $1 \leq \mathcal{M} \leq 3$ accurately describes the majority of the stellar interior models used.

sound speed are set equal to each other in equation (8), the solution for the Keplerian velocity is

$$v_\phi^2 = \pm \frac{(\mathcal{M}^3 \xi)^{1/2} G m_{comp} \beta^{3/2}}{r\left(\beta^2 + \mathcal{M}^{-2}\right)}. \quad (9)$$

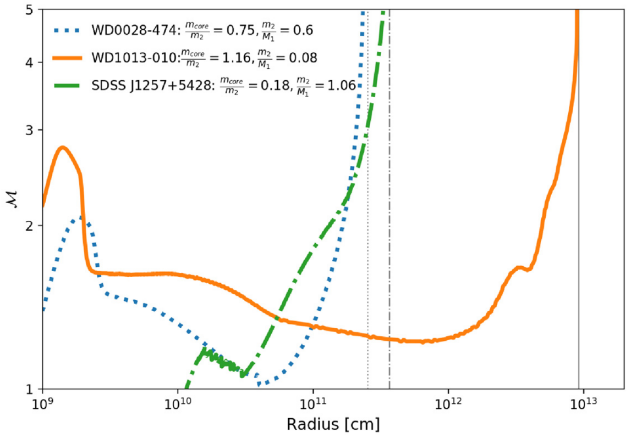

Figure 9. Mach number versus radius for three representative models. The dashed, blue curve follows the Mach number through a primary star of mass $1.0\,M_\odot$ with core mass $0.45\,M_\odot$ and companion of mass $0.6\,M_\odot$, closely representing the WD0028−474 system. The solid, orange curve follows the Mach number through a primary star of mass $5.0\,M_\odot$ with core mass $0.44\,M_\odot$ and companion of mass $0.38\,M_\odot$, closely representing the WD1013−010 system. The dot–dashed, green curve follows the Mach number through a primary star of mass $1.0\,M_\odot$ with core mass $0.2\,M_\odot$ and companion WD of mass $1.06\,M_\odot$, closely representing the SDSS J1257+5428 system. The grey vertical lines mark the outer radius of each primary star. The Mach values fall in the range $1 < \mathcal{M} < 3$ for all mass ratios in this work except where they asymptotically increase at the surface of the star.

Since the Keplerian velocity is a function of M_1, this equality can be expressed in terms of the mass ratio (m_{comp}/M_1), β, and $\mathcal{M}$ in the following way:

$$\frac{m_{comp}}{M_1} = \frac{\beta^2 + \mathcal{M}^{-2}}{(\mathcal{M}^3 \xi \beta^3)^{1/2}}. \quad (10)$$

The vast majority of β values are bounded by the above equation evaluated at $\mathcal{M} = 1$ and 3; these values are representative of the upper and lower limits of the Mach numbers within the primary's envelope. A plot of the above function in comparison to the relationship β versus m_{comp}/M_1 is shown in Fig. 8.

6 CONCLUSION

We considered how the effects of convection and spin-up in CE evolution impact the formation of DWDs. For each observed DWD system, two corresponding CEs were modelled: (i) the more-massive WD as the companion and the less massive WD as the core mass, and (ii) the less-massive WD as the companion and the more massive WD as the core mass. To study convective effects, we employ detailed stellar interior models to compare the convective transport time-scale to the inspiral time-scale and the drag luminosity to the maximum luminosity that can transport energy via subsonic convection. The stellar envelopes are spun up such that convection can accommodate the energy as the orbit decays. Our major findings are as follows:

(i) The correlation between the convective boundary and observed DWD separations reinforces the connection between short-period binaries and convective properties of the primary described in Wilson & Nordhaus (2019) (see Fig. 3).

(ii) Our physically motivated description of ejection efficiency, which combines convective effects with spinning up the convective region of the envelope, produces final separations of modelled systems that match observations of DWDs (see Fig. 7).

(iii) In order for convection to transport the energy released as the orbit decays, the envelope must be moderately spun up. The $v_{\rm env}/v_{\phi}$ values range from 0.0 to 0.82, with a peak between 0.5 and 0.7; the envelope is never required to spin-up faster than 82 per cent of the Keplerian speed to transport the full amount of orbital energy released during inspiral.

There are several promising directions for extending this work. Our physically motivated ejection efficiency could be included in population synthesis models. In particular, it would be interesting to see how Fig. 7 changes when the physics described in this work are incorporated into a binary population synthesis code with a proper IMF. High-resolution, global simulations of CEs do not include convection and radiation, both necessary ingredients for the effects described herein. Given that RGB/AGB stars possess deep and vigorous convective zones, future numerical work could be focused on incorporating these effects in self-consistent ways.

ACKNOWLEDGEMENTS

ECW and JN acknowledge support from the following grants: NASA HST-AR-15044, NTID SPDI15992, and NSF AST-2009713. The authors thank Noam Soker, Warren Brown, Na'ama Hallakoun, Gabriel Guidarelli, Silvia Toonen, Carles Badenes, Ashley Ruiter, Luke Chamandy, Eric Blackman, and Adam Frank for stimulating discussions.

DATA AVAILABILITY

No new observational data were generated from this research; data underlying this paper are available in the articles and supplementary materials of the referenced papers. Stellar interior models were derived from MESA (Modules for Experiments in Stellar Astrophysics), which is available at http://mesa.sourceforge.net.

REFERENCES

Badenes C., Mullally F., Thompson S. E., Lupton R. H., 2009, ApJ, 707, 971
Bloecker T., 1995, A&A, 297, 727
Bours M. C. et al., 2014, MNRAS, 438, 3399
Bours M. C. P. et al., 2015, in Duffour P., Bergeron P., Fontaine G., eds, ASP Conf. Ser. Vol. 493, White Dwarfs. Astron. Soc. Pac., San Francisco, p. 313
Brown W. R., Kilic M., Prieto C. A., Kenyon S. J., 2011, MNRAS, 411, L31
Brown W. R., Gianninas A., Kilic M., Kenyon S. J., Prieto C. A., 2016, ApJ, 818, 155
Brown W. R. et al., 2020, ApJ, 889, 49
Canals P., Torres S., Soker N., 2018, MNRAS, 480, 4519
Chamandy L. et al., 2018, MNRAS, 480, 1898
Chandrasekhar S., 1933, MNRAS, 93, 390
Chen Z., Frank A., Blackman E. G., Nordhaus J., Carroll-Nellenback J., 2017, MNRAS, 468, 4465
Cummings J. D., Kalirai J. S., Tremblay P.-E., Ramirez-Ruiz E., Choi J., 2018, ApJ, 866, 21
Davis P. J., Kolb U., Willems B., 2010, MNRAS, 403, 179
Debes J. H., Kilic M., Tremblay P. E., López-Morales M., Anglada-Escude G., Napiwotzki R., Osip D., Weinberger A., 2015, AJ, 149, 176
De Marco O., Passy J.-C., Moe M., Herwig F., Low M.-M. M., Paxton B., 2011, MNRAS, 411, 2277
Fabrycky D., Tremaine S., 2007, ApJ, 669, 1298
Ferrario L., 2012, MNRAS, 426, 2500
Glanz H., Perets H. B., 2018, MNRAS, 478, L12
Grichener A., Sabach E., Soker N., 2018, MNRAS, 478, 1818
Guidarelli G., Nordhaus J., Chamandy L., Chen Z., Blackman E. G., Frank A., Carroll-Nellenback J., Liu B., 2019, MNRAS, 490, 11179
Hallakoun N. et al., 2016, MNRAS, 458, 845
Hamada T., Salpeter E. E., 1961, ApJ, 134, 683
Holberg J. B., Saffer R. A., Tweedy R. W., Barstow M. A., 1995, ApJ, 452, L133
Iaconi R., de Marco O., 2019, MNRAS, 490, 2550
Iben Icko J., 1990, ApJ, 353, 215
Iben Icko J., Livio M., 1993, PASP, 105, 1373
Iben I. J., Tutukov A. V., 1984, ApJ, 284, 719
Ivanova N., 2018, ApJ, 858, L24
Ivanova N. et al., 2013, A&AR, 21, 59
Ivanova N., Justham S., Podsiadlowski P., 2015, MNRAS, 447, 2181
Jones D., 2020, in Kabáth P., Jones D., Skarka M., eds, Reviews of Modern Astrophysics, Observational Constraints on the Common Envelope Phase. Cham: Springer International Publishing, Switzerland AG, p. 123
Karl C., Napiwotzki R., Heber U., Lisker T., Nelemans G., Christlieb N., Reimers D., 2003a, in de Martino D., Silvotti R., Solheim J.-E., Kalytis R., eds, NATO ASIB Proc. Vol. 105, White Dwarfs. Kluwer, Napoli, p. 43
Karl C. A., Napiwotzki R., Nelemans G., Christlieb N., Koester D., Heber U., Reimers D., 2003b, A&A, 410, 663
Kashi A., Soker N., 2018, MNRAS, 480, 1
Kilic M., Brown W. R., Allende Prieto C., Pinsonneault M. H., Kenyon S. J., 2007a, ApJ, 664, 1088
Kilic M., Stanek K. Z., Pinsonneault M. H., 2007b, ApJ, 671, 761
Kilic M., Brown W. R., Prieto C. A., Swift B., Kenyon S. J., Liebert J., Agüeros M. A., 2009, ApJ, 695, L92
Kilic M., Brown W. R., Allende Prieto C., Kenyon S. J., Panei J. A., 2010, ApJ, 716, 122
Kilic M., Brown W. R., Hermes J. J., Gianninas A., 2015, in Sopuerta C. F., eds, Astrophysics and Space Science Proceedings, Vol. 40, Gravitational Wave Astrophysics. Springer, Switzerland, p. 167
Kochanek C. S., Adams S. M., Belczynski K., 2014, MNRAS, 443, 1319
Kruckow M. U., Tauris T. M., Langer N., Kramer M., Izzard R. G., 2018, MNRAS, 481, 1908
Kulkarni S. R., Van Kerkwijk M. H., 2010, ApJ, 719, 1123
Kuruwita R. L., Staff J., De Marco O., 2016, MNRAS, 461, 486
Livio M., Soker N., 1988, ApJ, 329, 764
MacLeod M., Cantiello M., Soares-Furtado M., 2018a, ApJ, 853, L1
MacLeod M., Ostriker E. C., Stone J. M., 2018b, ApJ, 863, 5
Maoz D., Hallakoun N., Badenes C., 2018, MNRAS, 476, 2584
Marsh T. R., 1995, MNRAS, 275, L1
Marsh T. R., 2011, Class. Quantum Gravity, 28, 95
Marsh T. R., Dhillon V. S., Duck S. R., 1995, MNRAS, 275, 828
Maxted P. F., Marsh T. R., Moran C. K., Han Z., 2000, MNRAS, 314, 334
Maxted P. F. L., Marsh T. R., Moran C. K. J., 2002a, MNRAS, 319, 305
Maxted P. F., Burleigh M. R., Marsh T. R., Bannister N. P., 2002b, MNRAS, 334, 833
Michaely E., Perets H. B., 2016, MNRAS, 458, 4188
Morales-Rueda L., Marsh T. R., Maxted P. F., Nelemans G., Karl C., Napiwotzki R., Moran C. K., 2005, MNRAS, 359, 648
Moran C., Marsh T. R., Bragaglia A., 1997, MNRAS, 288, 538
Mullally F., Badenes C., Thompson S. E., Lupton R., 2009, ApJ, 707, 51
Nandez J. L., Ivanova N., Lombardi J. C., 2015, MNRAS, 450, L39
Napiwotzki R. et al., 2002, A&A, 386, 957
Nelemans G. et al., 2005, A&A, 440, 1087
Nordhaus J., Blackman E. G., 2006, MNRAS, 370, 2004
Nordhaus J., Spiegel D. S., 2013, MNRAS, 432, 500
Nordhaus J., Blackman E. G., Frank A., 2007, MNRAS, 376, 599
Nordhaus J., Spiegel D. S., Ibgui L., Goodman J., Burrows A., 2010, MNRAS, 408, 631
Nordhaus J., Wellons S., Spiegel D. S., Metzger B. D., Blackman E. G., 2011, Proc. Natl. Acad. Sci., 108, 3135
Paczynski B., 1976, in Eggleton P., Mitton S., Whelan J., eds, Proc. IAU Symp. Vol. 73, Structure and Evolution of Close Binary Sytems. Kluwer, Dordrecht, p. 75
Park K., Bogdanović T., 2017, ApJ, 838, 103

Paxton B., Bildsten L., Dotter A., Herwig F., Lesaffre P., Timmes F., 2011, ApJS, 192, 3
Paxton B. et al., 2018, ApJS, 234, 34
Politano M., Weiler K. P., 2007, ApJ, 665, 663
Quataert E., Shiode J., 2012, MNRAS, 423, 92
Rebassa-Mansergas A., Parsons S. G., García-Berro E., Gänsicke B. T., Schreiber M. R., Rybicka M., Koester D., 2017, MNRAS, 466, 1575
Reichardt T. A., De Marco O., Iaconi R., Chamandy L., Price D. J., 2020, MNRAS, 494, 5333
Reimers D., 1975, Mem. Soc. R. Sci. Liege, 8, 369
Ricker P. M., Taam R. E., 2008, ApJ, 672, L41
Ricker P. M., Taam R. E., 2012, ApJ, 746, 74
Ruiter A. J., Belczynski K., Benacquista M., Larson S. L., Williams G., 2010, ApJ, 717, 1006
Sabach E., Hillel S., Schreier R., Soker N., 2017, MNRAS, 472, 4361
Saffer R. A., Liebert J., Olszewski E. W., 1988, ApJ, 334, 947
Santander-García M., Rodríguez-Gil P., Corradi R. L., Jones D., Miszalski B., Boffin H. M., Rubio-Díez M. M., Kotze M. M., 2015, Nature, 519, 63
Shappee B. J., Thompson T. A., 2013, ApJ, 766, 64
Shiode J. H., Quataert E., 2014, ApJ, 780, 96
Soker N., 2013, New Astron., 18, 18
Soker N., 2015, ApJ, 800, 114
Soker N., Grichener A., Sabach E., 2018, ApJ, 863, L14
Steinfadt J. D., Kaplan D. L., Shporer A., Bildsten L., Howell S. B., 2010, ApJ, 716, L146
Thompson T. A., 2011, ApJ, 741, 82
Toonen S., Nelemans G., 2013, A&A, 557, A87
Toonen S., Hollands M., Gänsicke B. T., Boekholt T., 2017, A&A, 602, A16
Tutukov A., Yungelson L., 1979, in Conti P., de Loore C., eds, Proc. IAU Symp. Vol. 83, Mass Loss and Evolution of O-Type Stars. Kluwer, Dordrecht, p. 401
Van Der Sluys M. V., Verbunt F., Pols O. R., 2006, A&A, 460, 209
Vennes S. et al., 2011, ApJ, 737, L16
Webbink R. F., 1984, ApJ, 277, 355
Wilson E. C., Nordhaus J., 2019, MNRAS, 485, 4492
Wood M. A., 1990, PHD thesis, Univ. Texas
Wood M. A., 1994, White Dwarfs. Springer, Berlin
Woods T. E., Ivanova N., Van Der Sluys M. V., Chaichenets S., 2012, ApJ, 744, 12
Zorotovic M., Schreiber M. R., Gänsicke B. T., Nebot Gómez-Morán A., 2010, A&A, 520, 86

This paper has been typeset from a TEX/LATEX file prepared by the author.